

passageways of these specimens. Additionally, because values for cross-sectional areas of the theropod nasal passages lie on or below the reptilian allometric regression (Fig. 3), respiratory turbinates were probably also absent in life. Similarly, CAT scans from a particularly well-preserved skull of the ornithischian dinosaur *Hypacrosaurus* (Ornithopoda: Hadrosauridae) also show no evidence of the presence of respiratory turbinates (Fig. 2F). Nasal cross sectional area in *Hypacrosaurus* is also coincident with the reptilian allometric regression (Fig. 3).

The proximity of the nostrils to the choanae (internal nares) in the maniraptoran theropod *Dromaeosaurus* (Dromaeosauridae) (12) and probably in *Deinonychus* (Dromaeosauridae) (13) as well is reminiscent of nasal cavity proportions in a variety of modern lizards (Varanidae, for example) (Fig. 5) (14). As in extant lizards, the abbreviated nasal passage associated with such a direct path of airflow into the oral cavity of these dinosaurs almost certainly precluded sufficient space in the nasal cavity to have accommodated respiratory turbinates.

Together the data indicate that a variety of Cretaceous theropod dinosaurs, and at least one genus of ornithischian dinosaurs, possessed crocodile- or lizardlike, relatively constricted nasal passages, devoid of sufficient cross-sectional area to have accommodated respiratory turbinates and endothermic-lung ventilation rates. These observations do not necessarily either preclude or support the possibility that some or all of the taxa investigated here maintained routine metabolic rates somewhat greater than those of extant ectotherms.

REFERENCES AND NOTES

1. J. H. Ostrom, in *The Dinosauria*, D. B. Weishampel, P. Dodson, H. Osmolka, Eds. (Univ. of California Press, Berkeley, CA, 1990), pp. 269–279.
2. A. Feduccia, *Naturwissenschaften* **80**, 564 (1993).
3. J. A. Ruben, *Annu. Rev. Physiol.* **57**, 69 (1995); J. F. Hubert et al., *J. Sediment. Res.* **66**, 531 (1996).
4. J. R. Spotila, M. P. O'Connor, F. V. Paladino, *Mod. Geol.* **16**, 203 (1991).
5. J. O. Farlow, P. Dodson, A. Chinsamy, *Annu. Rev. Ecol. Syst.* **26**, 445 (1995).
6. W. J. Hillenius, *Evolution* **48**, 207 (1994).
7. ———, *Paleobiol.* **18**, 117 (1992).
8. J. A. Ruben, in *Animals and Temperature*, I. A. Johnston and A. F. Bennett, Eds. (Cambridge Univ. Press, London, in press).
9. The rare exceptions in endotherms where respiratory turbinates are particularly poorly developed or absent are clearly related to secondary nasal or rostral specializations that preclude their presence. For example, turbinates and nostrils are absent in a number of diving birds of the order Pelecaniformes, including gannets, gannets, and cormorants. Most of these birds are plunge divers and anterior open nostrils would be a potential liability in such cases [J. D. MacDonal, *Proc. Zool. Soc. London* **135**, 357 (1960)]. Similarly, respiratory turbinates are also absent or poorly developed in whales. However, in these exceptions, the presence of compensatory mechanisms serves to emphasize that endothermic lung ventilation rates necessitate some adap-

10. L. M. Witmer, *J. Morphol.* **225**, 269 (1995).
11. K. A. Nagy and C. C. Peterson, *Ecol. Monogr.* **57**, 111 (1988).
12. P. J. Currie, *J. Vertebr. Paleontol.* **15**, 576 (1995).
13. J. H. Ostrom, *Bull. Am. Mus. Nat. Hist.* **30**, 1 (1969).
14. T. S. Parsons, in *Biology of the Reptilia*, C. Gans, d'A. Bellairs, T. S. Parsons, Eds. (Academic Press, New York, 1970), vol. 2, pp. 99–191.
15. Nasal cross-sectional areas were determined by means of microcomputer image analysis (MCID, Imaging Research, St. Catherines, Ontario, Canada) either of cranial CAT-scan imagery or directly from sectioned skulls.
16. P. Dodson, personal communication.
17. D. B. Weishampel, *J. Paleontol.* **55**, 1046 (1981).

18. J. A. Gauthier, *Calif. Acad. Sci. Mem.* **8**, 1 (1986).
19. We thank R. Aldred; P. Beardsley; V. Buchouse; P. Constant; S. Hamilton; M. Mason; A. Stuempl; S. Vondersaar; M. Woo; L. Yao; Children's Hospital, San Diego, CA; Good Samaritan Hospital, Corvallis, OR; and Salem Hospital, Salem, OR, for CAT scanning; D. Auth for the loan of varanid specimens; A. Bennett, P. Dodson, and D. Weishampel for comments; B. Byrne, J. Melville, and P. Murtaugh for statistical advice; J. Farlow for review and comments; J. Joslin and C. Simpkins of the Washington Park Zoo for donation of the varanid specimen; M. Mauxpoux for image analysis; M. Meers for advice; F. Moore and C. Richardson for equipment and advice; R. Pickton for bird specimens; G. Smith and N. Smith for donation of emu specimens; G. Vaillancourt and D. Vaillancourt for donation of ostrich specimens; and the University of California, Los Angeles, Dickey Collection; the Los Angeles County Museum of Natural History; and the Department of Zoology at Oregon State University for specimens. Supported by NSF grant IBN-9420290 to W.J.H. and J.A.R.

24 May 1996; accepted 24 June 1996

Enforcing Coherent Evolution in Dissipative Quantum Dynamics

J. I. Cirac, T. Pellizzari, P. Zoller

The major obstacle to the preparation and manipulation of many-particle entangled states is decoherence due to the coupling of the system to the environment. A scheme to correct for the effects of decoherence and enforce coherent evolution in the system dynamics is described and illustrated for the particular case of the ion-trap quantum computer.

The preparation and manipulation of N -particle entangled states is fundamental to the investigation of basic aspects of quantum mechanics and is the basis of applications such as quantum computation, teleportation, cryptography, and spectroscopy (1, 2). The major obstacle to the production of an entangled state in the laboratory is decoherence because the system couples to an environment. Suppressing environmental effects is thus essential to create entangled states in mesoscopic systems. This question is closely related to the problem of error correction in quantum computers (QC). In the following we adopt a language in which the manipulation of a system of particles is phrased as a computation in a QC. Such a device can be thought of as a system of spin-1/2 particles (qubits) with states $|0\rangle$ and $|1\rangle$. Any unitary (reversible) operation on the system of particles (that is, any computation) can be decomposed into a sequence of one-qubit or two-qubit gates, which are operations that involve one and two particles, respectively. Thus, any state (entangled or not) of the system can be generated if one can implement one- and two-qubit operations (1).

The effects of decoherence correspond to errors in the computation.

The error correction schemes proposed so far have focused on preserving a given entangled state (memory errors) (3). We introduce a method to correct for the effects of decoherence in the dynamical process of preparation and modification of entangled states (gate errors). The proposed scheme is a first-order error correction that allows us to effectively square the number of gate operations relative to the uncorrected case. The motivation is that in quantum optical systems, entangled states are achieved by coupling qubits to another degree of freedom that in turn undergoes decoherence by coupling to a heat bath. For example, in the ion-trap QC (4), the qubits can be stored in long-lived atomic ground states (5) with decoherence time ≈ 1000 s (2). Two-bit quantum gates are implemented by coupling the ions to the collective center-of-mass motion in the trap, which decoheres in a time ≈ 1 ms (5). Thus, at least in present experiments, gate errors predominate.

We illustrate our scheme in the context of the ion-trap QC (4). We consider a specific model of decoherence that results from a linear Markovian coupling between the ion motion (phonons) and a reservoir at

Institut für Theoretische Physik, Universität Innsbruck, Technikerstraße 25, A-6020 Innsbruck, Austria.

zero temperature. The essential results are summarized in Fig. 1, where we plot the fidelity for successful operation p as a function of the number of applied two-bit gates. Note that the number of reliable gates N_{op} is effectively squared.

The ideal (error free) evolution of a system during a two-qubit gate is governed by the Schrödinger equation $d/dt|\Psi_i(t)\rangle = -iH_0|\Psi_i(t)\rangle$, so that the quantum state at time t_g after the gate is $|\Psi_i(t_g)\rangle = U_0(t_g)|\Psi(0)\rangle$, where U_0 is the time evolution operator due to the Hamiltonian H_0 . We denote by \mathcal{H} the Hilbert space of input states $|\Psi(0)\rangle$, which coincides with the space of the possible output states $|\Psi_i(t_g)\rangle$. Environmental coupling causes the state of the system no longer to be pure but to develop into a mixture described by a system density operator ρ . Provided that the correlation time of the environment is much shorter than the typical system evolution time, this density operator obeys a Markovian master equation

$$\frac{d\rho}{dt} = -iH_{\text{eff}}\rho + i\rho H_{\text{eff}}^\dagger + \mathcal{F}\rho \quad (1)$$

where

$$H_{\text{eff}} = H_0 - i\sum_{j=1}^d \kappa_j a_j^\dagger a_j, \quad \mathcal{F}\rho = 2\sum_{j=1}^d \kappa_j a_j \rho a_j^\dagger \quad (2)$$

Here a_j are system operators as they appear in the system-environment coupling, whereas κ_j is related to the decoherence rate in the j th of d channels and \dagger denotes the Hermitian conjugate. These damping and noise terms introduce errors into the computation. The solution to the master equation after the gate can be expanded as $\rho(t_g) = |\Psi_i(t_g)\rangle\langle\Psi_i(t_g)| + \epsilon\rho_\epsilon + o(\epsilon^2)$, where $\epsilon = \max(\kappa_j t_g) \ll 1$ and ρ_ϵ is the first-order error. Thus, the number of gate operations N that can be successfully performed in the presence of decoherence is $N = o(1/\epsilon)$. We describe an error correction scheme that

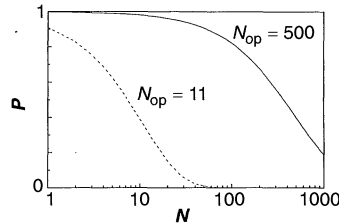


Fig. 1. Probability of measuring the correct result P_{ex} after the application of N two-bit quantum gates $C_{ab}^L: |e_1\rangle_a |e_2\rangle_b \rightarrow (-1)^{\epsilon_1 \epsilon_2} |e_1\rangle_a |e_2\rangle_b$ to the initial state $\propto |0\rangle_a |0\rangle_b + |1\rangle_a |1\rangle_b$. Dashed line: quantum gate without error correction. Solid line: present error-correcting scheme. The parameters have been chosen such that the probability for an error within a single gate C_{ab}^L without error correction is $p = 0.09$.

eliminates the effects of decoherence up to first order in ϵ and will square the number of possible operations: $N = o(1/\epsilon^2)$. We identify the conditions for this dynamical first-order error correction and show that this scheme can be implemented in a particular but relevant example of decoherence: a universal quantum gate in the ion-trap QC.

Although one could solve Eq. 1 up to first order in ϵ , we find it more convenient to use the language of quantum trajectories (6). In this case, the system evolution is represented by an ensemble of wave functions that propagate according to the effective Hamiltonian H_{eff} , interrupted at random times by quantum jumps. After the gate and up to order ϵ , the (normalized) system wave function will be either

$$|\Psi_j(t_g)\rangle = U_0(t_g - \tau) a_j U_0(\tau) |\Psi(0)\rangle / \|\cdot\| \quad (3)$$

in case of a jump at the random time $0 < \tau \leq t_g$ in channel j , or

$$|\Psi_{\text{Nj}}(t_g)\rangle = U_{\text{eff}}(t_g) |\Psi(0)\rangle / \|\cdot\| \approx |\Psi_i(t_g)\rangle + \epsilon |\Psi^\perp(t_g)\rangle \quad (4)$$

if no jump occurred. Here $\|\cdot\|$ denotes the norm, U_{eff} is the time-evolution operator generated by H_{eff} , and we have decomposed the state vector $|\Psi(t_g)\rangle$ into two orthogonal states: the first representing the ideal (error free) evolution $|\Psi_i(t_g)\rangle$, and the second, the error $|\Psi^\perp(t_g)\rangle$. Both the effective evolution and quantum jumps induce errors.

The idea of our first-order error correction scheme after the gate operation is as follows: First, perform a measurement \mathcal{M}_1 to detect whether a jump took place or not. If a jump is detected, apply a correction mechanism to recover the initial state and repeat the gate. For reasons that will be apparent below, this correction mechanism will involve another measurement \mathcal{M}_2 . If no jump occurred, perform an appropriate measurement \mathcal{M}_3 that projects onto the ideal state with probability $1 -$

$o(\epsilon^2)$. Let us now show in more detail the steps and conditions required for this method to work.

A) In order to detect unambiguously the occurrence of a jump with the measurement \mathcal{M}_1 , it is required that $|\Psi_j(t_g)\rangle \in \mathcal{H}_j \perp \mathcal{H}$.

B) If a jump is detected, we wish to restore the initial state $|\Psi(0)\rangle$. We do not know at which time τ during the gate the jump occurred, and therefore, the correction procedure has to restore the state regardless of the unknown (random) time τ . Obviously, this restoration cannot be achieved by a unitary evolution. Instead, one can use the projection postulate of quantum mechanics, that is, perform another measurement \mathcal{M}_2 to accomplish a non-unitary transformation. Depending on the outcome of this measurement, the state $|\Psi_j(t_g)\rangle$ will be projected onto a subspace $\mathcal{H}_j \subset \mathcal{H}$. In order to recover the state $|\Psi(0)\rangle$ uniquely, these spaces have to be mutually orthogonal and contain sufficient information to allow reconstruction of the original state.

C) In case of no jump, we wish to find a measurement \mathcal{M}_3 that restores the ideal state with probability $1 - o(\epsilon^2)$. This can be done provided that $|\Psi^\perp(t_g)\rangle \in \mathcal{H}_\perp \perp \mathcal{H}$. If this is fulfilled, the measurement \mathcal{M}_3 corresponds to a projection onto either \mathcal{H} or \mathcal{H}_\perp . The probability for projection onto the wrong state is $o(\epsilon^2)$.

These three conditions seem to be restrictive and difficult to satisfy in practice. However, we illustrate with an example how this procedure can be implemented for a particular model of quantum computation and decoherence. The ion-trap QC consists of a set of ions in a linear trap. Two internal atomic levels store the qubits. Single-qubit gates can be performed by acting with a resonant laser beam on the corresponding ion. Two-qubit gates are implemented by entangling two ions through the exchange of a phonon with a laser tuned to the lower motional side band (dim arrow in Fig. 2A).

Table 1. Two-qubit gate (Eq. 5) in the presence of phonon damping. Columns (i) to (iii) list the intermediate states during the steps in Eq. 5. The last column shows the unnormalized states (up to first order in ϵ) after the complete gate operation under H_{eff} (when no jump has taken place). The coefficients c_j and s_j are cosine and sines corresponding the Rabi oscillations in the j th step, respectively, for steps (i) to (iii). If there is no jump, the unnormalized state after the gate evolved according to H_{eff} [$\alpha_{1,2,3}$ are constants of order $o(1)$, depending on the ratio between Rabi frequencies for steps (i) and (ii)]. The boxes indicate the components of the states that survive after a quantum jump.

State	Step (i)	Step (ii)	Step (iii)	No jump
$ 00\rangle 0\rangle_p$	$ 00\rangle 0\rangle_p$	$ 00\rangle 0\rangle_p$	$ 00\rangle 0\rangle_p$	$ 00\rangle 0\rangle_p$
$ 01\rangle 0\rangle_p$	$ 01\rangle 0\rangle_p$	$ 01\rangle 0\rangle_p$	$ 01\rangle 0\rangle_p$	$ 01\rangle 0\rangle_p$
$ 10\rangle 0\rangle_p$	$c_1 10\rangle 0\rangle_p + \boxed{s_1 00\rangle 1\rangle_p}$	$\boxed{ 00\rangle 1\rangle_p}$	$\boxed{c_3 00\rangle 1\rangle_p} - s_3 10\rangle 0\rangle_p$	$e^{-\epsilon\alpha_1} 10\rangle 0\rangle_p + \alpha_3 00\rangle 1\rangle_p + o(\epsilon^2)$
$ 11\rangle 0\rangle_p$	$c_1 11\rangle 0\rangle_p + \boxed{s_1 01\rangle 1\rangle_p}$	$\boxed{c_2 01\rangle 1\rangle_p}$	$\boxed{-c_3 01\rangle 1\rangle_p} + s_3 11\rangle 0\rangle_p - s_2 0e^i\rangle 0\rangle_p$	$-e^{-\epsilon\alpha_2} 11\rangle 0\rangle_p + o(\epsilon^2)$

A universal two-bit quantum gate between ions a and b can be carried out in three steps (4): (i) a π laser pulse swaps the qubit of the ion a to the center-of-mass mode, (ii) a conditional sign change is introduced through an auxiliary state $|e'\rangle$ with the help of a 2π pulse on ion b , and (iii) the qubit of ion a is restored by inverting step (i). This corresponds to the sequence

$$C_{ab} : |\epsilon_1\rangle_a |\epsilon_2\rangle_b |0\rangle_p \xrightarrow{(i)} |0\rangle_a |\epsilon_2\rangle_b |\epsilon_1\rangle_p \xrightarrow{(ii)} (-1)^{\epsilon_1 \epsilon_2} |0\rangle_a |\epsilon_2\rangle_b |\epsilon_1\rangle_p \xrightarrow{(iii)} (-1)^{\epsilon_1 \epsilon_2} |\epsilon_1\rangle_a |\epsilon_2\rangle_b |0\rangle_p \quad (5)$$

where $|\epsilon_{1,2} = 0, 1\rangle_{a,b}$ represents the state of the ion, and $|n\rangle_p$ refers to phonons in the center-of-mass motion.

To illustrate how the correction scheme can be implemented, we assume that the phonons of the center-of-mass mode are coupled to a zero-temperature reservoir, as described by Eq. 1, with a single decoherence channel ($d = 1$), and where a is the phonon annihilation operator. Physically, this decoherence is the result of the coupling of the ion charge to the electrodes of the trap, which play the role of an environment (2). The effects of quantum jumps and the effective Hamiltonian during the gate (Eq. 5) are shown in Table 1.

The error-corrected quantum gate is based on the following three elements (Fig. 3):

1) At the beginning of the gate operation between ions a and b , we encode each of the logical (L) qubits in two physical qubits $a_{1,2}$ and $b_{1,2}$, respectively (redundant encoding)

$$|\epsilon\rangle_x \xrightarrow{\mathcal{U}} |\epsilon\rangle_x^L \otimes |\epsilon\rangle_x^R \equiv |\epsilon\rangle_{x_1} |0\rangle_{x_2} + |1-\epsilon\rangle_{x_1} |1\rangle_{x_2} \quad (6)$$

with $\epsilon = 0, 1$ and $x = a, b$; after the gate, we decode. These two physical qubits are stored in a single four-level ion $|0\rangle_x \equiv |0\rangle_{x_1} |0\rangle_{x_2} \dots$ (Fig. 2B). The unitary transformation \mathcal{U} thus requires only a single-ion operation. In addition, these “qubits” can be manipulated independently with single-ion operations (laser pulses). The Hilbert space of allowed computational inputs \mathcal{H} is spanned by states of the form

$$|\Psi(0)\rangle = \sum_{\epsilon_1, \epsilon_2=0,1} |\epsilon_1\rangle_a^L |\epsilon_2\rangle_b^L |0\rangle_p |\chi_{\epsilon_1, \epsilon_2}\rangle \quad (7)$$

where $|\chi\rangle$ denotes states of the rest of the ions not involved in the gate operation. They contain all of the information about the state of the QC.

2) Our aim is to perform the universal gate $C_{ab}^L : |\epsilon_1\rangle_a^L |\epsilon_2\rangle_b^L \rightarrow (-1)^{\epsilon_1 \epsilon_2} |\epsilon_1\rangle_a^L |\epsilon_2\rangle_b^L$ between the logical qubits a and b stored in the physical qubits $a_{1,2}$ and $b_{1,2}$, respectively. Using Eq. 6, we decompose $C_{a,b}^L = C_{a_2, b_1} C_{a_1, b_2} C_{a_2, b_2} C_{a_1, b_1}$ (Fig. 3). Each of these four subgates is now performed in the same

way as in the uncorrected case (Eq. 5). For reasons outlined below, we now use intermediate states involving two phonons $|2\rangle_p$. This can be achieved by tuning the laser to the second lower sideband (black arrow in Fig. 2A). Each of the four subgates C_{a_i, b_j} acts only on two physical qubits at a time. As an example we consider the operation C_{a_1, b_1} . The state of the QC Eq. 7 before the subgate can be rearranged as

$$|\Psi(0)\rangle = \sum_{\epsilon_1, \epsilon_2=0,1} |\epsilon_1\rangle_a |\epsilon_2\rangle_b |0\rangle_p |R_{\epsilon_1, \epsilon_2}\rangle \quad (8)$$

with

$$|R_{\epsilon_1, \epsilon_2}\rangle = |0\rangle_{a_2} |0\rangle_{b_2} |\chi_{\epsilon_1, \epsilon_2}\rangle + |0\rangle_{a_2} |1\rangle_{b_2} |\chi_{\epsilon_1, 1-\epsilon_2}\rangle + |1\rangle_{a_2} |0\rangle_{b_2} |\chi_{1-\epsilon_1, \epsilon_2}\rangle + |1\rangle_{a_2} |1\rangle_{b_2} |\chi_{1-\epsilon_1, 1-\epsilon_2}\rangle \quad (9)$$

The subgate C_{a_1, b_1} operates on only the first three kets of Eq. 8. The action of C_{a_1, b_1} (and the corresponding errors due to quantum jumps and the effective evolution) can be read directly from Eq. 5 and Table 1 with the replacement $|1\rangle_p \rightarrow |2\rangle_p$. Analogous arguments apply to the other subgates.

3) Measurements after the gate will involve detection of the presence or absence of phonons. This detection can be accomplished with an extra ion and the quantum jump technique (5). This “red light ion” is pumped into an additional internal level, provided that one or more phonons are present, by tuning a laser to the lower motional sideband. Fluorescence (the red light) will indicate the presence of phonons and thus an error.

Steps A through C outlined above are performed explicitly as follows (Fig. 3):

A_{ion}) According to Table 1, a quantum jump during one of the subgates will transform the state of the QC into a state with one phonon (wiggly line in Fig. 2A). This defines \mathcal{H}_j , which is orthogonal to \mathcal{H} as required in step A. The state after the jump will remain unaffected until the end of the subgate (independent of the jump time). Thus, the occurrence of a jump can be detected with the red light ion after the subgate, which defines the measurement \mathcal{M}_1 .

B_{ion}) If a jump was detected after one of the subgates, we wish to recover the state before this particular operation. As an ex-

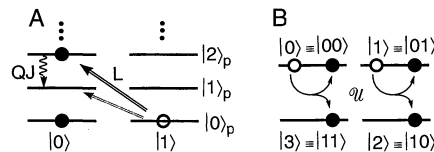


Fig. 2. (A) Step (i) of Eq. 5: tune the laser (L) to the first (dim arrow) or second (black arrow) motional sideband. Occurrence of a quantum jump is indicated by QJ. (B) Redundant encoding in a four-level ion as in Eq. 6.

ample, we show how this is accomplished for a quantum jump occurring in step (ii) (Table 1) of the subgate C_{a_1, b_1} . The resulting state will be

$$|\Psi_j\rangle \propto [\cos(\tau_2) |0\rangle_a |0\rangle_b |R_{1,0}\rangle + |0\rangle_a |1\rangle_b |R_{1,1}\rangle] |1\rangle_p \quad (10)$$

This state depends on the time τ_2 when the quantum jump occurred. However, this dependence can be eliminated by measuring the state of the physical qubit b_1 ; this action defines the measurement \mathcal{M}_2 . If the qubit b_1 is found in $|0\rangle_{b_1}$, the state of the QC will be projected onto $|\Psi_j\rangle \propto |0\rangle_a |0\rangle_b |R_{1,0}\rangle$, whereas if it is found in $|1\rangle_{b_1}$, the state of the QC will be projected onto $|\Psi_j\rangle \propto |0\rangle_a |1\rangle_b |R_{1,1}\rangle$. The subspaces \mathcal{H}_{j1} and \mathcal{H}_{j2} associated with the two possible outcomes of \mathcal{M}_2 contain all of the states $|\chi_{i,j}\rangle$ (Eq. 9), are manifestly orthogonal, and thus conform to condition B.

C_{ion}) If no jump took place during the first subgate, the state of the QC under the effective time evolution is given by Eq. 8 with the replacement of $|\epsilon_1\rangle_a |\epsilon_2\rangle_b |0\rangle_p$ with the last column of Table 1. There will be a superposition of $|0\rangle_p$ and $|2\rangle_p$ phonon states. The measurement \mathcal{M}_1 will project onto the state $|0\rangle_p$ with probability $1 - o(\epsilon^2)$, and therefore, we only need to consider the zero-phonon component. From Eq. 8 and Table 1 it can be shown that (to order ϵ) the complete gate $C_{a,b}^L$ yields the following transformation

$$|\epsilon_1\rangle_a^L |\epsilon_2\rangle_b^L \xrightarrow{H_{\text{eff}}} (-1)^{\epsilon_1 \epsilon_2} [1 - \epsilon\alpha] |\epsilon_1\rangle_a^L |\epsilon_2\rangle_b^L + \epsilon |\Psi_{\epsilon_1, \epsilon_2}^\perp\rangle \quad (11)$$

where α is independent of $\epsilon_{1,2}$ and $\langle \Psi_{\epsilon_1, \epsilon_2}^\perp | \epsilon_1'\rangle_a^L |\epsilon_2'\rangle_b^L \rangle = 0$ for all $\epsilon_{1,2}, \epsilon_{1,2}'$. Therefore, $\mathcal{H}_\perp \perp \mathcal{H}$, as required in C. After the fourth subgate and decoding \mathcal{U}^{-1} (Eq. 6), the state $|\Psi^\perp(t_g)\rangle$ will correspond to the one in which at least one of the ions a and b is in the lower manifold spanned by $|1\rangle_{x_1} |0\rangle_{x_2}$ and $|1\rangle_{x_1} |1\rangle_{x_2}$ ($x = a, b$). The measurement \mathcal{M}_3 simply checks [with probability of success $1 - o(\epsilon^2)$] that no population is left within this manifold. This measurement is again implemented with the quantum jump technique.

The numerical results presented in Fig. 1 are based on the example discussed above.

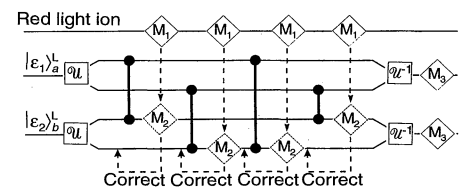


Fig. 3. Logical two-qubit gate with error correction.

We plot the probability to measure the correct result P after N applications of the gate C_{ab}^L to the initial state $|\Psi(0)\rangle \propto (|0\rangle_a^L|0\rangle_b^L + |1\rangle_a^L|1\rangle_b^L)$. We have chosen the parameters such that a single gate C_{ab}^L fails with probability $p = 0.09$. Without error correction (dashed line), $N_{\text{op}} \approx 1/p \approx 11$ gates can be performed reliably, where $P = \exp(-N/N_{\text{op}})$. Note that we have used the gate C_{ab}^L instead of C_{ab} (Eq. 5) for the uncorrected case to make comparison easier. With error correction we can perform $N_{\text{op}} \approx 4/p^2 \approx 500$ gates.

The present scheme can be generalized to more realistic situations. First, it is relevant to extend the present scheme to finite temperature reservoirs for the phonon mode. In this case, there are two decoherence channels corresponding to heating and cooling. To distinguish the corresponding quantum jumps, one has to use the third motional sideband and design \mathcal{M}_1 to measure the phonon number (7). Second, it is possible to correct for the occurrence of n quantum jumps in one decoherence channel (jump operator a) during one gate, which would allow $N = o(1/\epsilon^{n+1})$ operations. For this correction, one has to use the $n+1$ th sideband and gate symmetrization as in (8).

A remarkable feature of our proposal is that error-testing measurements are performed after the gate operation to correct errors that accumulated during the computation. The overhead required by the scheme is rather moderate: each logical qubit is encoded into two qubits that are stored in the same (four-level) ion. This setup has the advantage that one-qubit gates (for which decoherence is assumed to be negligible) are the same with or without the redundant encoding. On the other hand, implementation of the two-qubit gate requires an overhead of four two-qubit sub-gates. A proof-of-principle experiment to demonstrate the possibility of correcting effects of decoherence in dissipative quantum dynamics could be performed with three trapped ions, which seems to be attainable with present technology (5).

REFERENCES AND NOTES

1. C. H. Bennett, *Phys. Today* **48**, 24 (October 1995); D. P. DiVincenzo, *Science* **270**, 255 (1995).
2. D. J. Wineland *et al.*, *Phys. Rev. A* **50**, 67 (1994).
3. P. W. Shor, *ibid.* **52**, 2493 (1995); I. L. Chuang, R. Laflamme, P. W. Shor, W. H. Zurek, *Science* **270**, 1633 (1995); A. Steane, preprint quant-ph/9605021 at <http://xxx.lanl.gov>; H. Mabuchi and P. Zoller, *Phys. Rev. Lett.* **76**, 3108 (1996); E. Knill and R. Laflamme, preprint quant-ph/9600034 at <http://xxx.lanl.gov>
4. J. I. Cirac and P. Zoller, *Phys. Rev. Lett.* **74**, 4091 (1995).
5. C. Monroe *et al.*, *ibid.* **75**, 4714 (1995).
6. J. Dalibard *et al.*, *ibid.* **68**, 580 (1992); C. W. Gardiner *et al.*, *Phys. Rev. A* **46**, 4363 (1992); H. J. Carmichael, *An Open Systems Approach to Quantum Optics*, Lecture Notes in Physics m18 (Springer,

- Berlin, 1993). For a review, see P. Zoller and C. W. Gardiner, in *Quantum Fluctuations*, Lecture Notes Les Houches Summer School 1995, E. Giacobino *et al.*, Eds. (Elsevier, New York, in press).
7. T. Pellizzari *et al.*, unpublished results.
 8. T. Pellizzari *et al.*, *Phys. Rev. Lett.* **75**, 3788 (1995).

9. This work is supported in part by the Austrian Science Foundation, Acciones Integradas Austria-Spain, and the European quantum information network.

19 April 1996; accepted 16 July 1996

Flux Line Lattice Melting Transition in $\text{YBa}_2\text{Cu}_3\text{O}_{6.94}$ Observed in Specific Heat Experiments

Marlyse Roulin, Alain Junod,* Eric Walker

When a magnetic field penetrates a type II superconductor, it forms a lattice of thin quantized filaments called magnetic vortices. Resistance, magnetization, and neutron diffraction experiments have shown that the vortex lattice of high-temperature superconductors can melt along a line in the field-temperature plane. The calorimetric signature of melting on this line was observed in a high-accuracy adiabatic specific heat experiment performed on $\text{YBa}_2\text{Cu}_3\text{O}_{6.94}$. The specific heat of the vortex liquid was greater than that of the vortex solid.

When the temperature T of a classical type II superconductor is lowered in a constant magnetic field $H > 0$, it enters a mixed state in which the field partially penetrates the sample and forms a lattice of thin quantized filaments called magnetic vortices. Each vortex carries a quantum of magnetic flux Φ_0 . Although the mixed state is superconducting, an electric current generates dissipation if the vortex lattice is allowed to flow. Fortunately, this lattice can be pinned and the zero-resistance (R) state restored (up to a critical current) by introducing suitable defects. In any case, the magnetization $M = -\partial F/\partial H$ (where F is the free energy) varies continuously at the border of the mixed state, and the transition is therefore of second order. The specific heat C shows a jump without any latent heat.

The magnetic structure that is obtained upon cooling most high-temperature superconductors through the superconducting phase boundary differs from this picture. The vortices first form a liquid. Although the discussion of the normal state to superconductivity is also controversial because of the effect of thermal fluctuations (1), the main interest has concentrated on the transition in the superconducting state—the freezing of the vortex lattice.

Vortex lattice freezing or melting has been investigated by several groups using mainly resistance, magnetization, and neutron diffraction experiments (2–7). Phase diagrams were constructed in the (H, T) plane and correspond to the usual (p, T) phase diagram

(where p is pressure) for solids and liquids made of atoms or molecules. An interesting difference is the possibility of varying the density of vortices over orders of magnitude by simply changing the magnetic field. The melting line for $\text{Bi}_2\text{Sr}_2\text{CaCu}_2\text{O}_8$ (Bi-2212) was found to join smoothly the superconducting transition temperature [$T_c = 90$ K, induction field $B = 0$] and a critical point ($T_{\text{cr}} = 37.8$ K, $B_{\text{cr}} = 380$ G) (3). Hall probes revealed a jump in M that increased from $4\pi\Delta M \approx 0.2$ G just above T_{cr} to ≈ 0.4 G just below T_c . In $\text{YBa}_2\text{Cu}_3\text{O}_7$ (Y-123), the melting line could be followed from the superconducting transition temperature ($T_c = 93$ K, $B = 0$) up to the point ($T = 78$ K, $B = 8$ T) (5, 6). The possible existence of a critical point at higher fields was not clarified. A jump in M was also observed with SQUID (superconducting quantum-interference device) magnetometry that decreased smoothly from $4\pi\Delta M \approx 0.3$ G at 82 K to zero at T_c (5, 6). These jumps in M in both Bi-2212 and Y-123 were considered as a thermodynamic argument in favor of a first-order transition.

The full proof for the existence of a first-order transition at the melting temperature $T_m(H)$ must include the observation of the corresponding discontinuity in the entropy $S = -\partial F/\partial T$, or equivalently, of a peak in C with an integrated latent heat $\Delta Q = T_m\Delta S$. Because the number of vortices is directly proportional to the induction field B , then, due to the much higher melting fields in Y-123, it should be possible, for a given temperature near T_c , to observe an effect that is about two orders of magnitude greater for Y-123 than for Bi-2212; therefore, we focused on Y-123. The Clausius-Clapeyron equation, $\Delta S/\Delta M = -dH_m/dT$,

Département de Physique de la Matière Condensée, Université de Genève, CH-1211 Genève 4, Switzerland.

*To whom correspondence should be addressed.